Optical Performance of Roman Optical Telescope Assembly

Bente H. Eegholm[a,1], Josh Johnson[b], Peter Miller[b], Josh Abel[a], Matt Bolcar[a], Bill Castle[b], Boris Glebov[c], Alden Jurling[a], Pete McCarthy[b], Elise Michaels[b], Scott Paine[b], Malcolm O'Sullivan[b], Karen Gorski[b], and Jeffrey Scott Smith[a].

[a]NASA Goddard Space Flight Center, Greenbelt, MD 20771
[b]L3Harris Corporation, 1350 Jefferson Road, Rochester, NY 14623
[c]Peraton, Inc., Goddard Space Flight Center, Greenbelt, MD 20771

ABSTRACT

The Roman Space Telescope is a three mirror anastigmat design with a 2.4 m primary mirror, which will provide science information on dark energy and exoplanets via two science instruments. The Optical Telescope Assembly (OTA) was aligned at ambient temperature in a vacuum chamber. Following a vibration test, the OTA's optical performance, wavefront error, and pupil alignment, were tested at cold operational temperatures in a thermal vacuum chamber. Both test campaigns were performed in double-pass configuration, employing interferometry, Focus Diverse Phase Retrieval, and Shack-Hartman Wavefront Sensing test techniques. Alignment adjustments during the tests were made to the actuated Secondary Mirror, and Fold Mirror 1 in the Wide Field Instrument channel. Stability of the optical telescope assembly (OTA) is a critical need for Roman. For the TVAC test campaign, L3Harris and NASA developed a novel test with the objective of measuring the optical response of key parts of the OTA in the presence of small amplitude thermal stimuli; the Sinusoidal Thermoelastic Distortion Test (STDT). The basic concept is to use the flight hardware's own thermal control system to generate repeated thermal disturbances while continuously monitoring the optical response.

The telescope's predicted On-Orbit, End of Life quasi static optical wave front error performance is well within the required 67.3/74.2 nm RMS for the WFI/CGI channel.

Keywords: Telescope, optics, Roman, optical testing, Focus Diverse Phase Retrieval, FDPR, Sinusoidal Thermoelastic Distortion Test, STDT, alignment.

[1] Corresponding author: Bente Hoffmann Eegholm, E-mail: bente.h.eegholm@nasa.gov

1. INTRODUCTION

The Nancy Grace Roman Space Telescope (Roman) followed the James Webb Space Telescope (JWST) as NASA's next Astrophysics flagship mission. Roman will enhance the understanding of dark energy cosmology and exoplanet information, the accelerated expansion of the universe, and large-scale clustering of galaxies and dark matter. To achieve these scientific objectives, Roman's capabilities include a large field of view, which leads to challenges in testing the optical telescope.

The telescope is a three-mirror anastigmat design with a 2.4 m primary mirror, partly based on existing hardware and design heritage [1]. The telescope has two optical channels: one for the Wide Field Instrument (WFI), and one for the technology demonstration Coronagraph Instrument (CGI). The WFI channel enables the Wide Field Instrument to provide a field of view of more than 100 times larger than that of the Hubble Space Telescope WFC3-IR camera field of view, and with comparable sensitivity and spatial resolution [2], [3]. The WFI features a 288 megapixel near-infrared detector array providing a field of 0.8 degrees by 0.4 degrees. The WFI also provides spectroscopy capability [4], [5]. The CGI channel provides a collimated beam to the Coronagraph Instrument. Roman will operate in a libration orbit about the Sun-Earth L2 Lagrange point.

During 2024, the Optical Telescope Assembly (OTA) was aligned at ambient temperature in a vacuum chamber. Following acoustics and vibration testing, the OTA's optical performance, wavefront error, and pupil alignment were tested at cold operational temperatures in a thermal vacuum chamber. Both test campaigns were performed in double-pass test configuration, employing interferometry, Focus Diverse Phase Retrieval (FDPR), and Shack-Hartman Wavefront Sensing (SH-WFS) test techniques. Alignment adjustments during the test campaigns were made to the telescope Secondary Mirror and Fold Mirror 1 in the WFI channel.

Stability of the optical telescope assembly (OTA) is a critical need for Roman. For the TVAC test campaign, L3Harris and NASA developed a novel test with the objective of measuring the optical response of key parts of the OTA in the presence of small amplitude thermal stimuli; the Sinusoidal Thermoelastic Distortion Test (STDT). The basic concept is to use the flight hardware's own thermal control system [6] to generate repeated thermal disturbances while continuously monitoring the optical response.

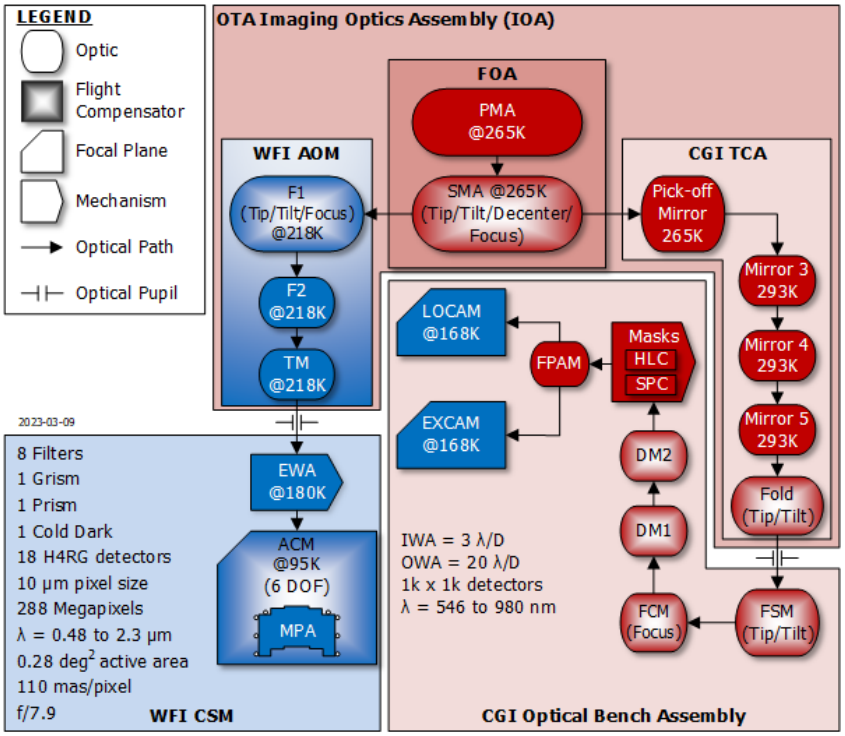

Figure 1. Block diagram of the Roman optical system

The Roman optical system block diagram is shown in Figure 1. The telescope has two optical paths, one for the WFI and one for the CGI. The telescope has focusing and alignment capability available on-orbit as well as on ground via three actuated mirrors. The mirror actuator range is dimensioned to be used both in ground alignment, as well as on orbit from commissioning through mission end-of-life.

The OTA consists of the Imaging Optics Assembly (IOA), and its associated Thermal Control Electronics (TCE) system. The TCE provides the temperature control of the IOA, as well as the interface to control the telescope mirror actuators. The TCE and thermal balance testing was part of the TVAC test campaign, but will not be discussed further is this paper, which focuses on optical performance. In the following, the word telescope will refer to the optical part of OTA, the IOA.

The Primary Mirror Assembly (PMA) and Secondary Mirror Assembly (SMA) are in the common path shared by the two instruments. The path is split into a dedicated channel with relay optics for each instrument. The SM is actuated in 5 Degrees Of Freedom (DOF); piston, tip, tilt, x-decenter, and y-decenter. The motion is controlled by the Alignment Drive (AD) system (hexapod), and focus adjustments are performed via the Focus Drive (FD) linear actuator system.

Invar growth and composite moisture desorption are affecting the OTA throughout its lifecycle. These two EOL effects cause near-pure defocus of the OTA wave front error (WFE), and most of that defocus is common to both the Wide Field and Coronagraph channels. To maintain optical performance on orbit, periodic focus adjustments are necessary. Less frequently, the OTA will need a more thorough re-alignment.

The WFI receives its input via the IOA Aft-Optics Module (AOM). AOM consists of two flat fold mirror assemblies (FM1A and FM2A) and a tertiary mirror assembly (TMA). FM1A is actuated in 3 DOF; piston, tip, and tilt, capable of compensating focus and pupil shear. The CGI receives its collimated input via the 5-mirror IOA Tertiary Collimator Assembly (TCA), which consists of a flat mirror in the pick-off mirror assembly (POMA), and a tertiary opto-mechanical assembly (TOMA) containing three powered optics (M3, M4, M5). TOMA collimates the beam and projects a pupil into CGI via the flat tip/tilt fold (TTF) mirror. The TTF is actuated in 2-DOF (tip and tilt) to control the pupil image location in CGI.
Figure 2 shows an optical ray trace through the system with the WFI channel to the right and the CGI channel to the left. Figure 3 shows the IOA and labels to the relevant parts.

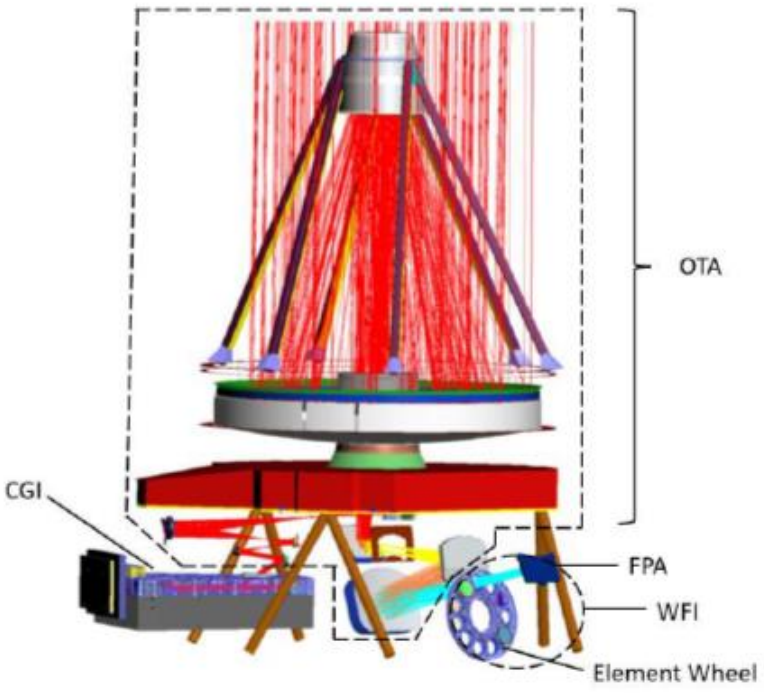

Figure 2. Optical ray trace of the Roman IPA

This paper describes the optical test, alignment, and performance of the telescope, hereinafter called the IOA for Integrated Optics Assembly, which is the optical telescope alone, not including the two science instruments. The verification plan [7] was designed to provide the individual optical performance of the telescope and the two science instruments before they were integrated. The end-to-end test of Roman is taking place at NASA Goddard Space Flight Center after integration.

Each of the individual telescope mirrors were optical performance tested interferometrically before integration and alignment into the next assembly level. Two of the mirrors, the PM and the TM also individually underwent optical performance testing with interferometry at ambient and cold temperatures in a TVAC chamber. L3Harris performed optical cold-shift tests on the two most impactful optics at the assembly level and correlated the subsystem Finite Element Models (FEM) that were included in the telescope. At the final telescope assembly stage, IOA underwent two large optical test campaigns; an alignment and performance test in a vacuum chamber, and an optical performance test at cold and hot operational temperatures in a thermal vacuum chamber. This is the test campaign described in this paper.

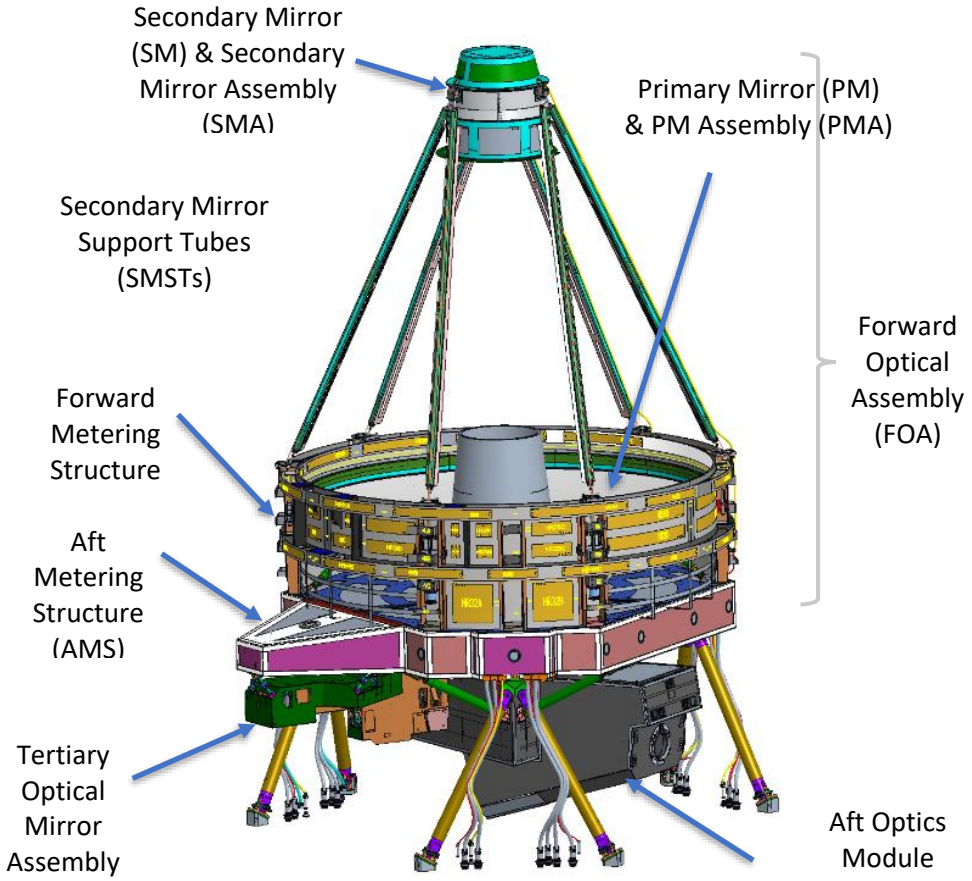

Figure 3 IOA overview

2. AMBIENT ALIGNMENT AND TESTING

The initial integration and alignment of the Roman telescope was performed at ambient temperature and soft (~5-10 Torr) vacuum. The SMA was rough aligned to the Payload Coordinate System (PCS) via laser tracker and secondary mirror strut adjustments prior to installation in the test chamber. The actuated mirror FM1A in the WFI path was locked in place before the start of this alignment activity with the actuators at the center of their travel. The POMA single fold mirror in

the CGI path was already locked in place. The TOMA structure containing three powered mirrors and an actuated tip/tilt fold mirror (TTF) was aligned as a standalone box prior to the telescope alignment test, using a CGH to replicate the FOA.

Testing was done in a double-pass configuration from the image plane of the WFI and in the collimated output of the CGI path. A full aperture Autocollimating Flat (ACF) is installed in top of the chamber and tilted to return the test beam on itself for each measured field point [8].

The tests were performed without the instruments present. A Computer Generated Hologram (CGH) was used as an Image Surface Reference Fixture (ISRF) to properly locate the WFI image plane. The IOA is designed to be used at any field on the detector. Five representative field points (center and four corners) were selected for measurements during the ambient and TVAC tests for the WFI channel.

The CGH included fiducials that were referenced to alignment targets to allow for the measurement of the WFI pupil in space for diameter, location, and clocking. The CGI path used a Pupil Reference Fixture (PRF) to set the output angle of the CGI path and also included pupil references to allow for the measurement of the CGI pupil diameter, location, and clocking. The CGI was measured at one field point due to the extremely small field of view. Both the PRF and ISRF were characterized relative to alignment targets to enable accurate placement in the Payload Coordinate System (PCS) via laser tracker. The primary mirror (PM) utilized a gravity offloader for all interferometric testing to minimize the gravity sag of the mirror. The un-offloaded mirror has too much sag for interferometry to work in the double-pass test configuration as the mirror sag under gravity exceeds the dynamic range of double-pass interferometry.

Figure 4 shows the IOA inside the chamber in preparation for optical testing.

Figure 4 IOA in test chamber. CGI test equipment in front center, WFI test equipment in right rear.
Photo: NASA/Chris Gunn

Once the IOA was in the chamber, the FM2A and TMA were installed on hexapods and aligned via laser tracker to the PCS. These mirrors, along with the SMA, would be adjusted to align the WFI path during the test. Similarly, the TOMA location would be adjusted via shims to maximize CGI performance.

Further tests at soft vacuum were completed to minimize the WFE of the WFI with alignment corrections done with the SMA, TMA, and FM2A remotely using the SMA prime actuators and hexapods. The predicted temperature and gravity shifts in the IOA from the test conditions to the on-orbit conditions were compensated for during the alignment. The anticipated changes were determined using STOP (Structural Thermal Optical Performance) analysis. The goal was to have a system that will perform optimally on-orbit, which means that it is not perfect on the ground in the test, but once it gets on orbit it will have all the optics in the optimum location. Uncertainty in the analysis and test is carried in the WFE budget and included in the final predictions.

Once the performance of the system was optimized, the chamber was repressurized and the TMA and FM2A bonded in place. The TOMA was shimmed to align the CGI path. Finally, the SM struts were adjusted to maximize the actuator range available on orbit. Once the optics were in position, the chamber was again de-pressurized and final adjustments and measurements taken. Now the degrees of freedom available were the actuated SMA and FM1A, which were both adjusted to optimize both optical paths. Portions of the prime actuator range were preserved for the factory alignment to optimize performance. The final measured results for both fields are shown in Figure5. These plots are the average of three consecutive full tests. The maximum measured WFI error was 36.4 nm, which represents a margin increase of more than 20 nm in an RSS sense against the initial error budget coming into the alignment.

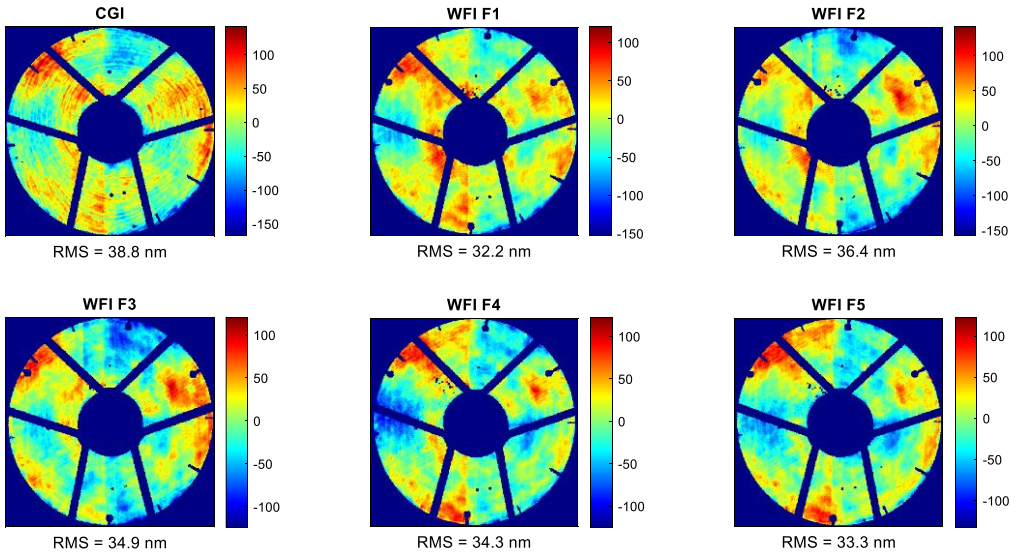

Figure 5 Final ambient measured wavefront error of the IOA. These values do not include uncertainty.

In addition to the interferometric data collected during the ambient test, Focus Diversity Phase Retrieval (FDPR) data for the WFI and Shack-Hartmann Wavefront Sensor (SH WFS) data for the CGI were also collected, both with the PM offloaded for gravity and with it un-offloaded. These tests were in preparation for the upcoming TVAC testing to be performed without off-loader, and with no interferometry data collected. Both methods of testing agreed with the interferometric tests of the appropriate path within uncertainty expectations.

3. FDPR TEST OVERVIEW

FDPR is used to measure wavefront error in the WFI path of the RST IOA, and a commercially available Shack-Hartmann wavefront sensor (SH-WFS) is used to measure the wavefront error in the CGI path. Analysis was done both with the PM offloaded for gravity and with it non-offloaded, in order to tie the interferometry results to the FDPR/SH-WFS results. For

the data where the PM was offloaded, the wavefront error measured via phase retrieval was compared to interferometry data to assess FDPR accuracy and calibrate the focus offset between the ISRF used for interferometry and the source camera modules (SCMs) used for FDPR. This information was used in preparation for the TVAC testing where the PM is non-offloaded.

Point-spread function (PSF) images were taken using a double-pass configuration for the WFI. Images were taken for each of the five field points also measured interferometrically. Each field point had a series of images taken through focus at five different SCM stage positions for the purposes of focus diversity, which improves phase retrieval performance. Starting estimates for the wavefront error were taken from a Code V model of the double-pass RST IOA which also provided alignment targets.

The Source Camera Module (SCM) test set is part of Optical Ground Support Equipment (OGSE) that implements the FDPR portion of the optical verification of Roman's Imaging Optics Assembly (IOA) telescope. The SCM test set provides the data necessary for quantitative evaluation of wavefront quality produced by the IOA via FDPR analysis.

4. FDPR DOUBLE-PASS TEST GEOMETRY AND COMPONENTS

An FDPR dataset comprises a series of images acquired at varying amounts of defocus. Analysis of these data yields the complex wavefront presented to the FDPR acquisition system. Combining the recovered wavefront with a model of the optical system that produced the wavefront provides information about the state of this optical system, such as alignment and quality of its components.

The IOA optical test was performed in a double-pass arrangement – with both the light source and the image acquisition hardware placed near the nominal system image plane. Light traverses the optical system twice. First "backwards," from the image plane into the collimated space. Then, after being returned by the Auto-Collimating Flat (ACF), it will traverse the optical system in the "forward" direction, at which point the FDPR images will be captured. In the ambient and TVAC test chambers used during the IOA testing the SCM is used, the ACF is hanging above the IOA. The ACF has a diameter which is larger than the PM. Tip-tilt control of the ACF allows capturing data from a variety of source points, and thus observation of a range of system field points. SCM components can be translated along the optical axis, providing the necessary defocus. The general operating principle is shown in Figure 6.

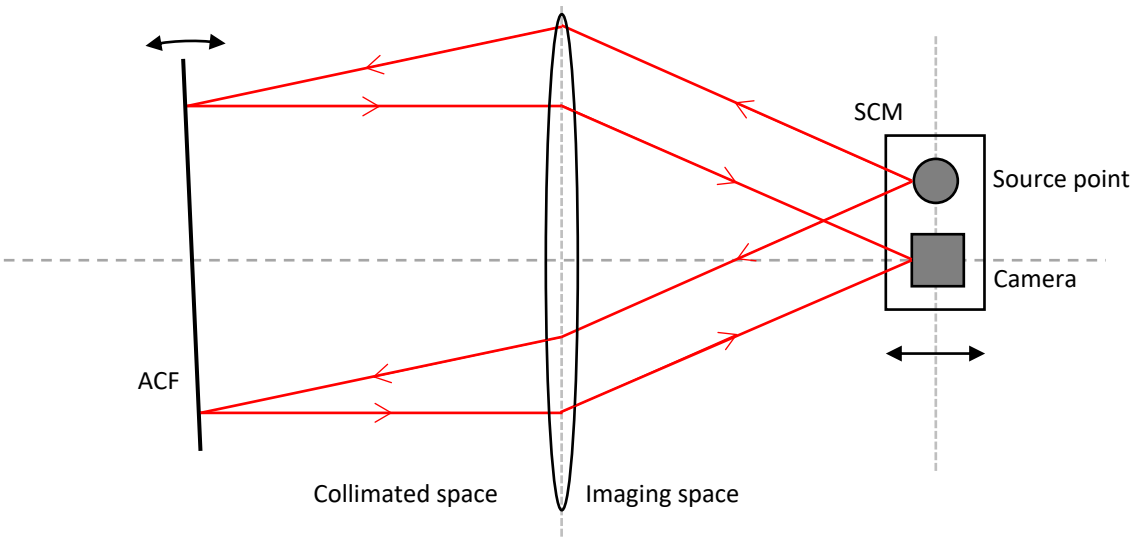

Figure 6 Schematic overview (not to scale) of FDPR data acquisition in double-pass geometry.

The SCM components were mounted on a hexapod. Its purpose is to maneuver the SCM components into appropriate positions and orientations relative to the IOA. Note that the SCM test set, not the hexapod, will provide the defocus movement needed for FDPR.

The SCM test set operates as a pulsed-exposure image capture system, and it provides the functionality of appropriately generating and conditioning the optical test signal, controlling the amount of defocus necessary for FDPR, injecting light into the telescope, and acquiring images of the light distribution returned by the IOA and the ACF. A schematic of the SCM is shown in Figure 7. The test set provides all the necessary controls for performing and monitoring these functions, as well as their automation for the purposes of collecting FDPR data. The SCM units are TVAC-compatible, requiring no enclosure. The source is a 633 nm CW laser, chopped to 1 ms pulses, 630HP single-mode fiber. The camera has a 2048x2048 sensor, with pixel size 5.5 µm, and 12-bit ADC. The SCM motion range is 10 mm, with an integrated position sensor (1 µm accuracy). Each SCM unit is fitted with closed-loop thermal regulator ensuring minimum safe operating temperature.

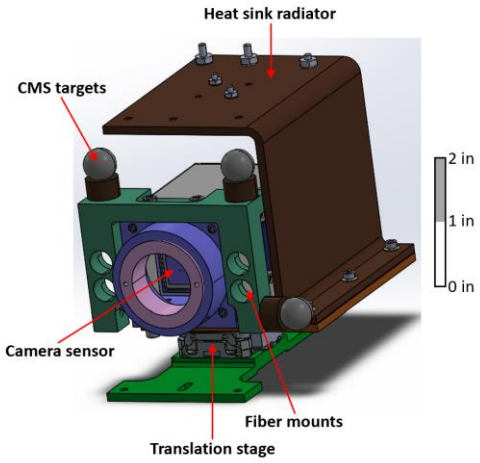

Figure 7 Schematic of the Source Camera Module (SCM).

Across all 5 field points, the difference between the wavefront from FDPR and interferometry was 15.12 nm RMS averaged across the field, with tip, tilt, and power removed. When considering low-order spatial frequencies (Zernikes up to 8th order), the agreement was on average 11.06 nm RMS, indicating that the 15.12 nm RMS average consists of 11.06 nm RMS of low-order error and 10.3 nm RMS of high-order error. It is important to note that we would not expect the FDPR wavefront to match interferometry exactly. FDPR is a non-common path test, so there will be different WFE due to the return beam traveling a slightly different path, especially on the AOM optics.

5. THERMAL VACUUM TEST

Following the ambient alignment, the IOA successfully underwent acoustic and vibration testing, which will not be covered here. The final optical performance test was the Thermal Vacuum (TVAC) testing done in L3Harris' Chamber A large vacuum chamber, capable of reaching 1e-7 Torr, and equipped with a thermal shroud and ACF for optical testing at flight-like temperatures. FDPR was used for the WFI path and the SH-WFS was used for the CGI path. With the exception of a different ACF, the test equipment was otherwise the same as the ambient test, and the two interferometers were still used to locate the field points and to collect pupil data for the test. Pupil data collection required adjusting the ACF to collect six images at slightly different tilts in order to cover the entire pupil, then stitching the resulting pictures together for pupil analysis.

Optical data was collected at various temperature plateaus during the TVAC test, with different temperature profiles across the IOA. See Figure 8 for the as- run profiles temperature averages for the different components in the IOA. All testing was done at hard vacuum at approximately 2e-7 Torr. The at ambient temperature were used as baseline for the cold shift measurements. After those tests, the IOA was brought to near-use temperature conditions in both Protoflight Cold (PFC) and Protoflight Hot (PFH) plateaus. The optical performance of the system was optimized by alignment adjustments of the SM and FM1A at PFC.

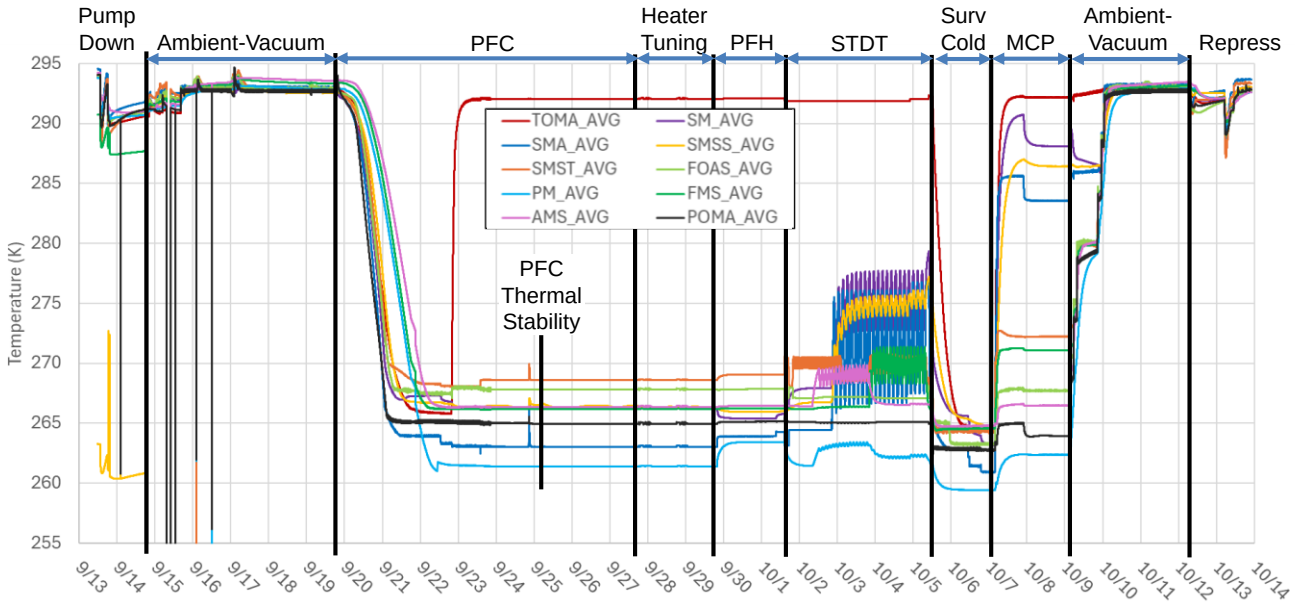

Figure 8 As-run thermal data showing component average temperatures.

From an optical perspective, the most important aspect of the TVAC test was to measure the change in wavefront as the system went from ambient temperature to flight-like temperatures. The ambient test, using interferometry and the PM gravity offloader, had much less signal to look through and was deemed a higher quality test. The WFE budget was constructed such that the interferometric test was the baseline measurement, to which would be added the cold shift from the TVAC test. This enabled the FDPR and SH WFS tests to be delta tests, where much of the test uncertainty could be removed from the budget as it would be common to both the ambient and flight-like temperature tests.

6. MEASURED RESULTS

The final average surface error maps for both the WFI and CGI paths, separated by plateau, at the IOA exit pupils, are shown in Figure 9 and Figure10. All measured WFEs shown are after analytical corrections to minimize WFE. These theoretical corrections use the actuated degrees of freedom including the SM (5 DOF), FM1A (3 DOF), and the image plane (2 DOF). All data for a given plateau is at a single pose of all actuators; there is no change for each individual field point or instrument, in order to mimic the on-orbit operation. This is to simulate alignment corrections made on orbit to optimize the performance using FDPR.

PROTOFLIGHT COLD

The initial cool-down to on-orbit conditions caused more WFE than expected, particularly in focus, but ultimately the error was largely correctable. Two alignment adjustments were made to minimize WFE and a third small analytical correction optimization was included in the results below. The third correction will be physically implemented during later TVAC testing at GSFC. The protoflight cold results are shown in Figure 11 and are the average of two complete tests, with no changes between them. The largest difference between the two tests was 25.4 nm RMS. The difference drops to 3.6 nm RMS with power removed. The data is being compared to the average of the pre- and post-TVAC ambient tests. One signature that can be seen in the cold shift is the frit effect of the SM, which looks like relatively large quilting in the maps, particularly visible in WFI F3 below as the red ‘bubbles’ in the WFE. A residual error from frit was predicted.

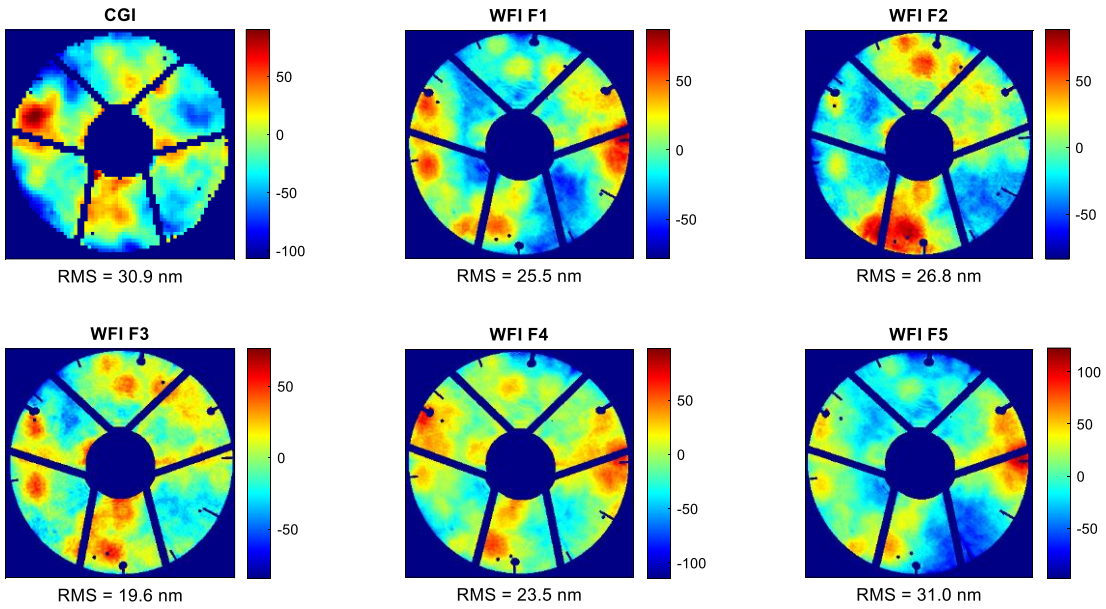

Figure 9 Change from ambient to Protoflight Cold after alignment corrections.

PROTOFLIGHT HOT

The Protoflight Hot plateau is largely the same as the PFC plateau as the heater setpoints for the IOA are the same with the difference being the temperature of the shroud surrounding the IOA. The measured WFE for PFH looks very similar to that of PFC. The PFH results are shown in Figure 10 and are the average of two tests with no alignment or actuator changes between them. The largest difference between the two tests was 14.6 nm RMS. The difference drops to 3.3 nm RMS with power removed.

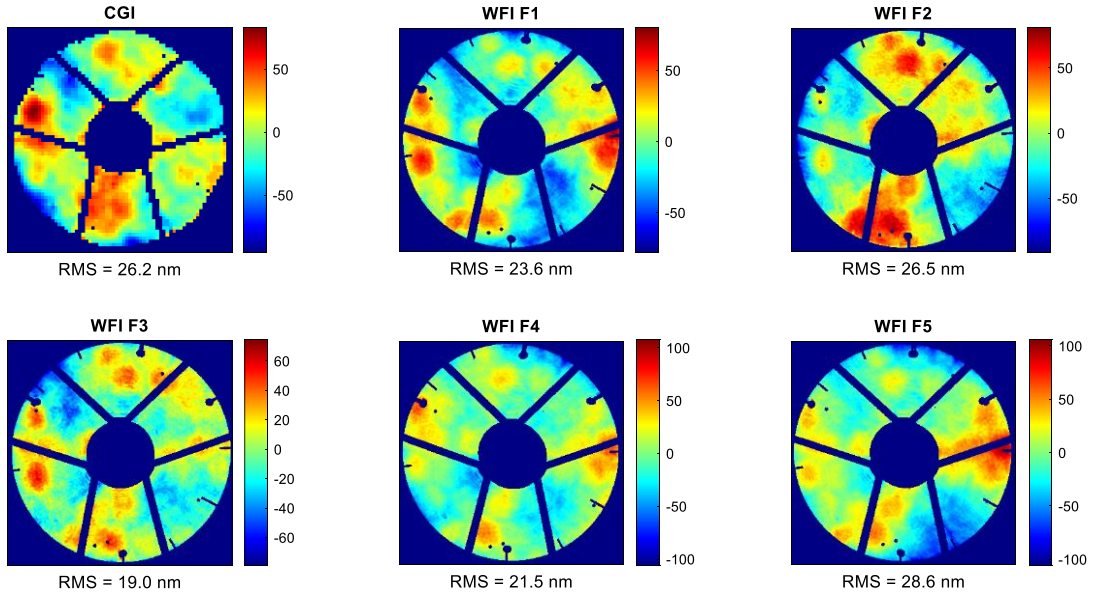

Figure 10 Change from Ambient to Protoflight Hot after small alignment correction.

PFC AND PFH AVERAGE

While this is not a separate plateau, it is useful to show the average of the PFC and PFH data in Figure 11. This represents the best estimate of the performance of the IOA in normal operating conditions, as both PFH and PFC exceed worst-case expected conditions in opposite directions in use. The data is being compared to the average of the pre- and post-TVAC ambient tests. The worst field is 29.5 nm RMS, which is included as the measured cold shift in the WFE budget. The results show a well aligned and compensated system, showing remaining uncorrectable residuals only, primarily from frit bonding.

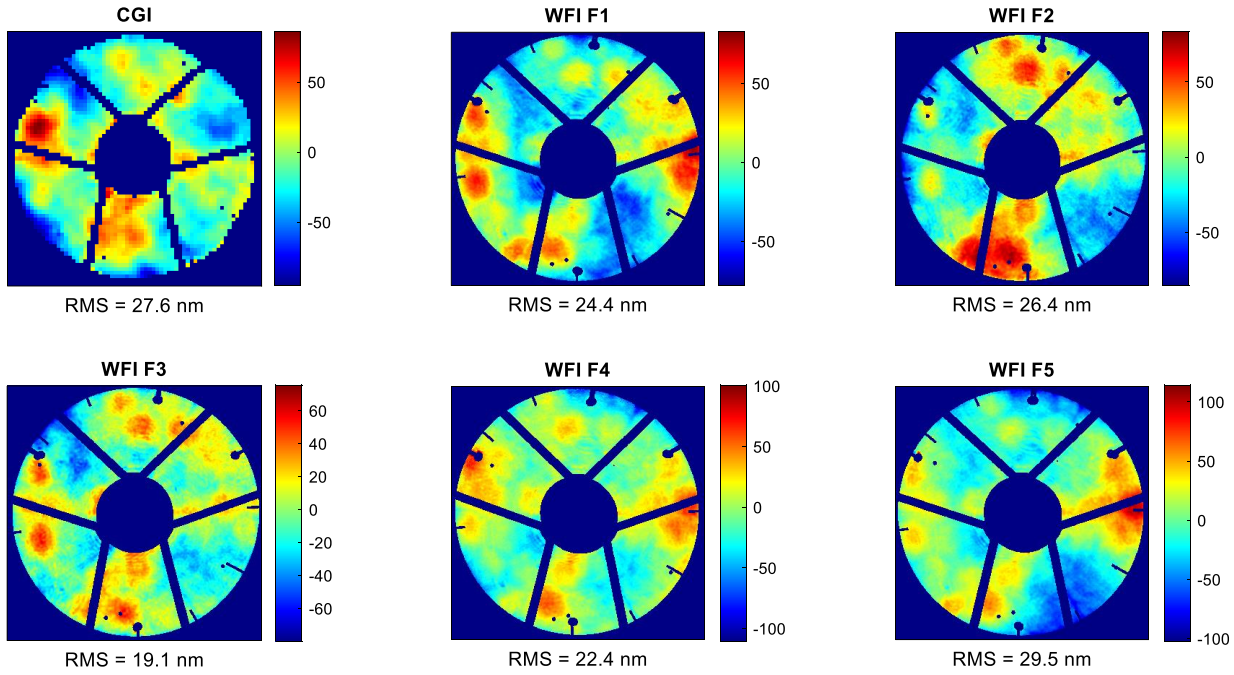

Figure 11 Average of PFC and PFH with alignment correction for best WFE.

7. PUPIL MEASUREMENTS

In addition to the WFE measurements, the pupil location, diameter, and clocking was measured for both ambient and TVAC tests. The WFI and CGI pupil locations and sizes are determined by fitting the geometry of the boresight intensity image. First, the intensity image needed to be stitched together due to the gravity sag of the PM. The interferometers cannot see the entire pupil at once, so six images were acquired, differing in the tilt of the ACF to illuminate different portions of the pupil. Figure 12 shows the stitched-together pupil measurement for the WFI.

Based on the stitched pupil image, the decenter and diameter analysis uses the pupil edge locations, fiducial locations on the ISRF/PRF, and the strut center line intersections with the pupil outer diameter to determine both the pupil shear and diameter. The clocking is determined after transforming the pupil image to a binary mask via thresholding, then comparing to a similarly created mask from the CodeV optical model.

The pupil shear measurements, pupil diameter measurements, and the clocking measurements for both paths at flight-like temperature were all acceptable.

After PFH, the Sinusoidal Thermoelastic Distortion Test (STDT) test was performed before transitioning to survival cold, where no optical testing was done.

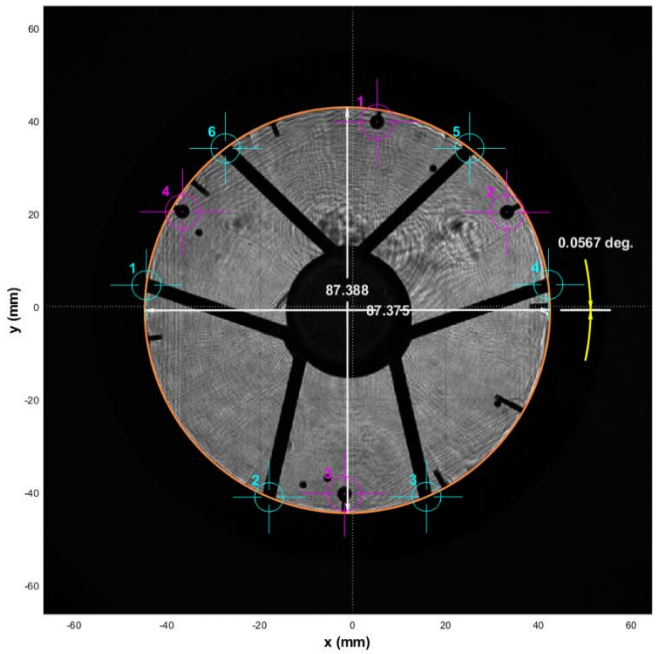

Figure 12 Example WFI pupil calculation result. This is from PFC.

8. SINUSOIDAL THERMAL DISTORTION TEST (STDT)

Stability of the optical telescope assembly is a critical need for the Roman program. The two light paths to the instruments (Widefield Instrument (WFI) and Coronagraph Instrument (CGI)) both need extremely stable and repeatable optical behavior to enable their science objectives. Both light paths have requirements for sub-nanometer wavefront stability over periods of minutes to hours. Because these sub-nm requirements cannot be directly measured and verified in test, they are verified by analysis using test-validated models. In order to validate the models for small amplitude thermoelastic behavior, it is desirable to test the hardware using thermal disturbances that are as small as can practicably be measured.

L3Harris and NASA developed a novel test with the objective of measuring the optical response of key parts of the OTA in the presence of small amplitude thermal stimuli. This test was called the Sinusoidal Thermoelastic Distortion Test (STDT). The basic concept is to use the flight hardware's own thermal control system to generate repeated thermal disturbances while continuously monitoring the optical response. Signal processing techniques can then be used to extract the optical response from the background noise. The result is that WFE responses with amplitudes well below the repeatability/precision level of a typical optical tests can be measured and compared against model predictions.

The flight thermal control system of the IOA was used to generate the thermal stimuli used during this test. The thermal stimulus is generated by updating the temperature setpoints in a predetermined pattern. This causes the thermal control system to try to follow the setpoint changes by changing the heater power outputs. This results in a temperature fluctuation on parts of the IOA. Several different areas of the IOA were chosen to be stimulated based on their predicted impact to optical stability. Figure 13 shows the thermal stimulus enacted for various pieces of hardware.

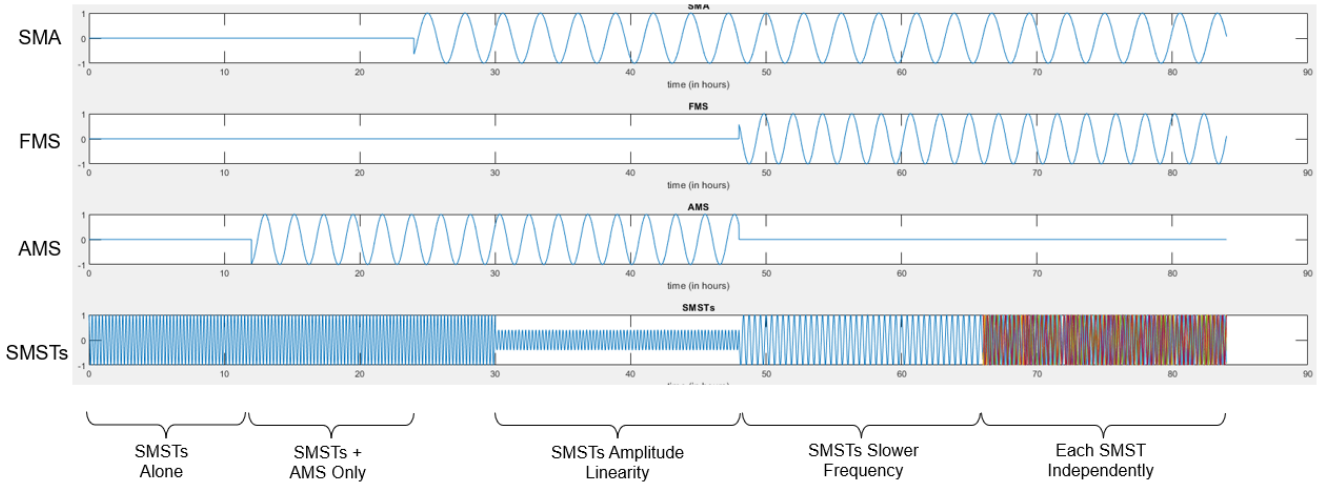

Figure 13 Thermal stimulus plan over the active duration of STDT.

FDPR wavefront sensing was used to monitor the optical response and generate WFE maps during the entirety of the thermal simului at a rate of one measurement per second. Following the test, analog signal processing techniques were used to extract the signal from background noise.

TEST RESULTS

Optical responses from all stimuli were successfully observed. While tip/tilt and power measurements were typically greater than one nm, higher order Zernike terms such as coma, trefoil, etc. were consistently measured at the sub-nm level. Principal component analysis (PCA) was used to assess the dominant WFE shapes associated with each stimulus, and amplitudes of Zernike terms were also calculated to compare to STOP modeling predictions. Figure 14 shows an example of the PCA analysis associated with the Aft Metering Structure (AMS) stimlulus/response. Shown at the top is the PCA component with the top 6 corresponding wavefront shapes listed, and below is the time series plot that shows the change in this term in blue alongside AMS temperature in orange. The PCA component has been multiplied by -1 in order to clearly show the correlation with temperature, otherwise the temperature line is not visible.

STOP MODEL CORRELATION AND VALIDATION

The STDT results showed that most of the stimuli resulted in smaller optical responses than STOP analysis predicted, confirming that STOP modeling is conservative in those areas of the telescope. However, two stimuli had greater than predicted optical responses. Considerable effort was put into investigating these underpredictions. In the end, both were determined to be caused by highly localized transient thermal gradients that needed greater model fidelity to predict these effects. The investigation also determined that this behavior would not be applicable to flight operating scenarios.

The STDT test also confirmed that the critically important coefficient of thermal expansion (CTE) on the secondary mirror support tubes (SMSTs) was within previous measurement uncertainties. The STDT test was able to show that the CTE of these tube assemblies was extraordinarily low (<20 ppb/K), and close to the predicted value. Results from this test enabled the team to fine tune the modeled strut assembly CTEs to more precisely predict on orbit behavior for this highly sensitive structure.

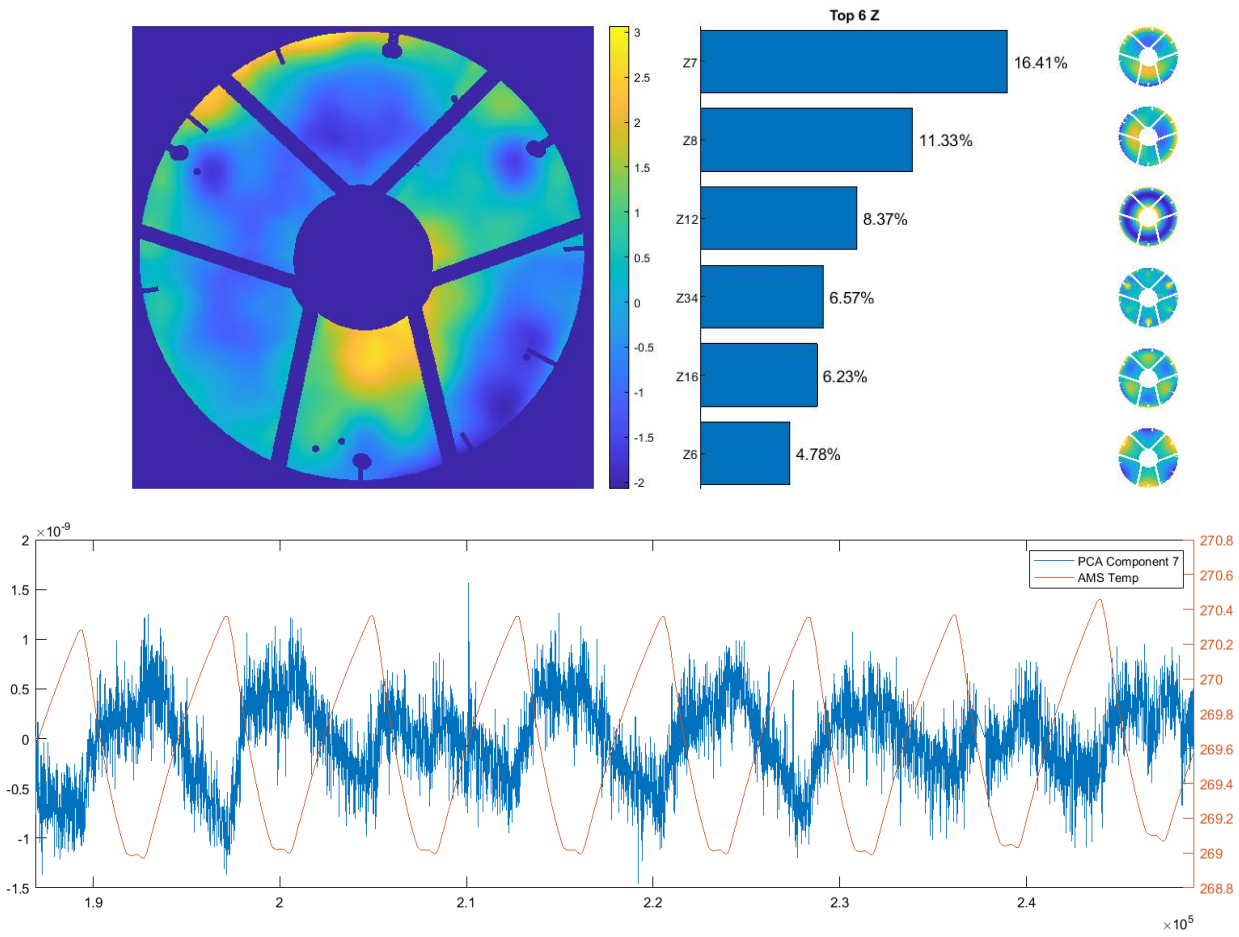

Figure 14 Unique AMS wavefront signature. Shown above is the PCA component with the top 6 corresponding wavefront shapes listed, and below is the time series plot that shows the change in this term in blue alongside AMS temperature in orange. The PCA component has been multiplied by -1 in order to clearly show the correlation with temperature, otherwise the temperature line is not visible.

9. ON ORBIT PERFORMANCE

PREDICTED QUASISTATIC ON-ORBIT PERFORMANCE

The predicted on-orbit performance takes results from the ambient temperature test as well as the TVAC test plateaus. The IOA measurement at ambient temperature, soft vacuum is added to the measured cold shift from the TVAC test, which uses the difference between the ambient temperature data and the average of the PFC and PFH data. The average of the two protoflight tests is being used because that is the best estimate of a typical environment in use on-orbit. The worst WFI field result of 44.5 nm RMS shown in Figure 15 goes into the WFE budget. The measured CGI WFE is 40.8 nm RMS. Note that no uncertainty is included in these plots and RMS values. When the uncertainty terms from the WFE budget are included, the WFI predicted performance is 61.8 nm against the 67.3 nm requirement, and the CGI predicted performance is 64.3 nm against the 74.2 nm requirement. Both paths show significant margin to the WFE budgets.

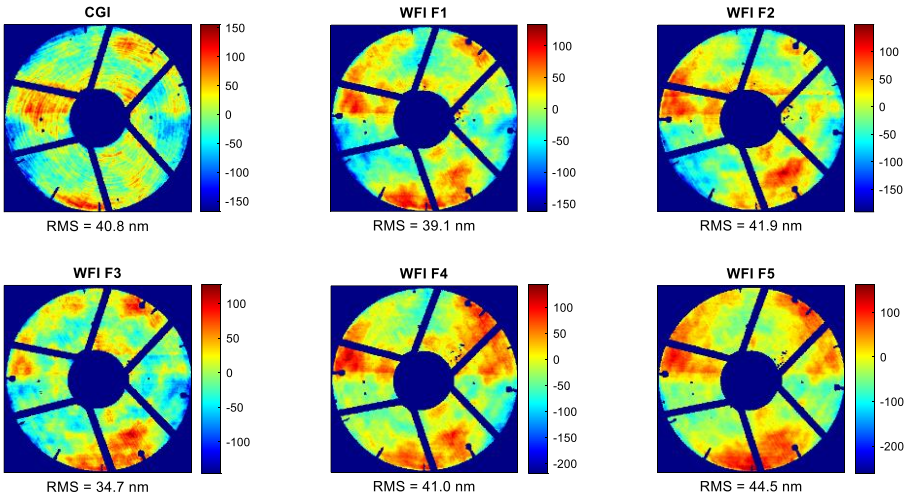

Figure 15 On-orbit best prediction for WFE. Uncertainty is not included.

The measured test results from both ambient and TVAC were used to create an as-built CodeV model of the IOA. The model differs from the measured results by 14.4 nm or less, which is within the uncertainty of the test data. The as-built model is calculated for 450 fields and used to determine the system performance at any point in the field and shows that the worst field point is only slightly higher than the measured values.

Figure 16 Test-correlated model WFI WFE vs FOV with design residual removed.

Figure 16 shows the WFE over the RST FOV of the correlated model, with excellent performance over the entire field.

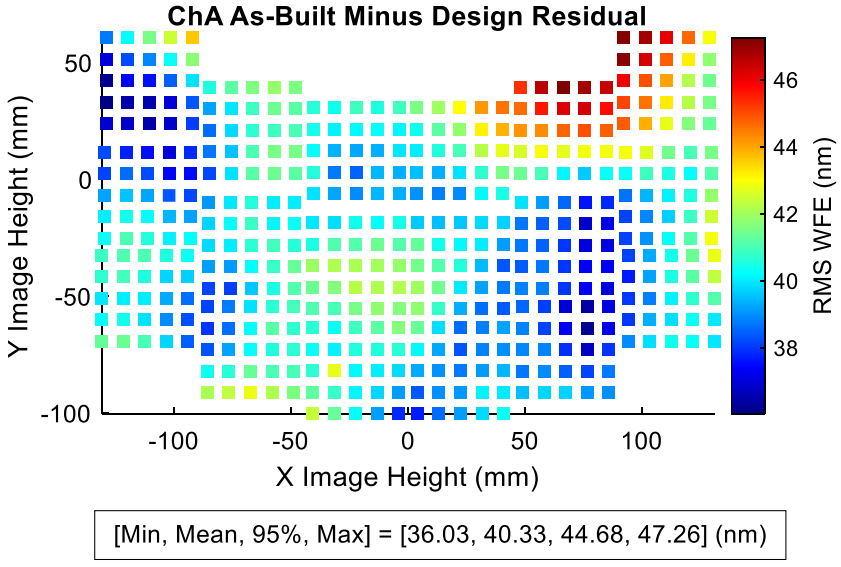

Figure 16 Test-correlated model WFI WFE vs FOV with design residual removed.

PREDICTED OPTICAL STABILITY PERFORMANCE

Optical stability is critical to the science goals of both instruments on this mission. The stability requirements are very tight (many are specified in picometers of WFE change), and the OTA team aggressively addressed this challenge throughout the program. This included the development of new composite materials with extraordinarily low CTEs, and the development of a new thermal control system capable of controlling to sub-milli-Kelvin temperature stability. The result is unprecedented optical stability for a large telescope.

On-orbit optical stability predictions are generated via STOP analysis using test validated models. A highly realistic thermal control algorithm is paired with correlated thermal, structural, and optical models to precisely simulate the behavior of the OTA. Two different operating scenarios are assessed for on orbit optical stability, one for each of the optical channels/instruments.

For widefield channel predictions, a very conservative "worst-case slew" scenario is used. This assumes an instantaneous slew and roll (from a thermal model perspective) between two parts of the field of regard that have the largest quasi-static delta, followed by 24 hours of static pointing at the new field of regard. No thermal stabilization period is used, meaning that the telescope is ready to take images throughout the entirety of the scenario with no downtime. Figures17a and 17b show predictions of the WFE stability during 3 min. and 2 hour sliding windows throughout the scenario. The plots show stability from shortly before the slew/roll event until 24 hours after it. The somewhat erratic-looking behavior seen in figure 17a is due to injecting a conservative amount of temperature sensing noise into each of the control loops. This conservative noise simulation is actually a significant driver of WFE stability predictions over shorter time frames. During this worst-case slew scenario, the 3 min. stability never exceeds 10 picometers, and the 2 hour stability never exceeds 200 picometers of WFE change. All widefield channel optical stability predictions are dramatically lower (better) than requirements, even when conservative Model Uncertainty Factors (MUFs) are applied. On-orbit behavior is expected to be even better than these predictions.

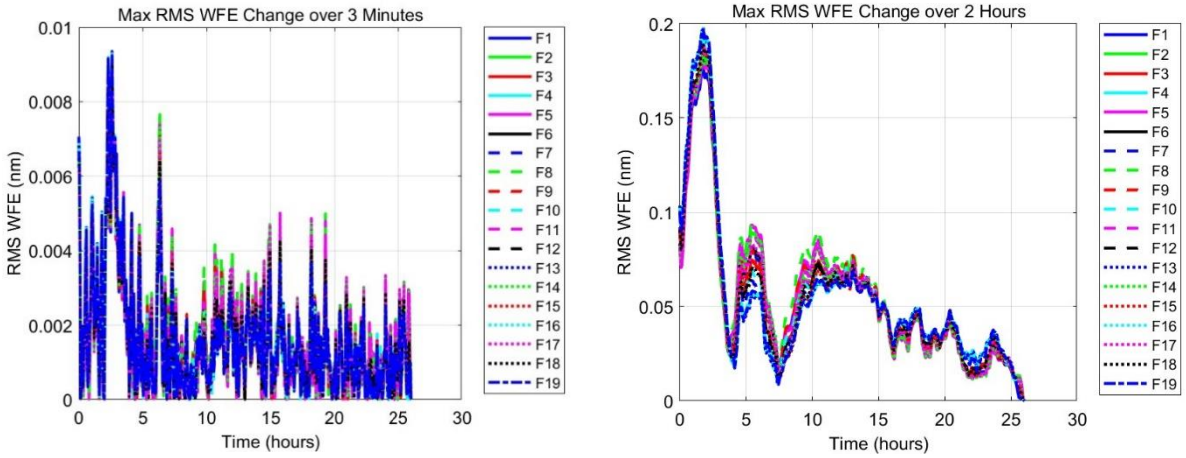

Figure 17 WFE changes at 19 different field points in the WFI channel over sliding 3 minute (a) and 2 hour (b) windows during worst-case slew scenario, starting just before the large slew/roll and continuing till 24 hours after the event.

For the Coronagraph channel, optical stability is assessed for a day-in-the-life scenario called OS11. This scenario involves simulating numerous slews back-and-forth between a reference star and the target star as well as rolls about the optical axis over a 100 hour duration. Figures18a and 18b show WFE stability over a sliding 10 hour window during this OS11 scenario. The pattern of the repeated humps present in the results is a result of repeated slews between the target star and the reference star. The results are split into Z4 (defocus) and Z5-Z11 (higher order Zernikes) because the coronagraph

instrument that is downstream of the telescope has a focus correction control loop that operates at a different rate than the CGI's deformable mirror, which would correct some of the higher order terms. The results shown here are before any WFE compensation is performed by the coronagraph instrument. Over this sliding 10 hour window, the WFE is predicted to change by less than 120 picometers of defocus, and less than 16 picometers of Z5-Z11. This is dramatically better than requirements.

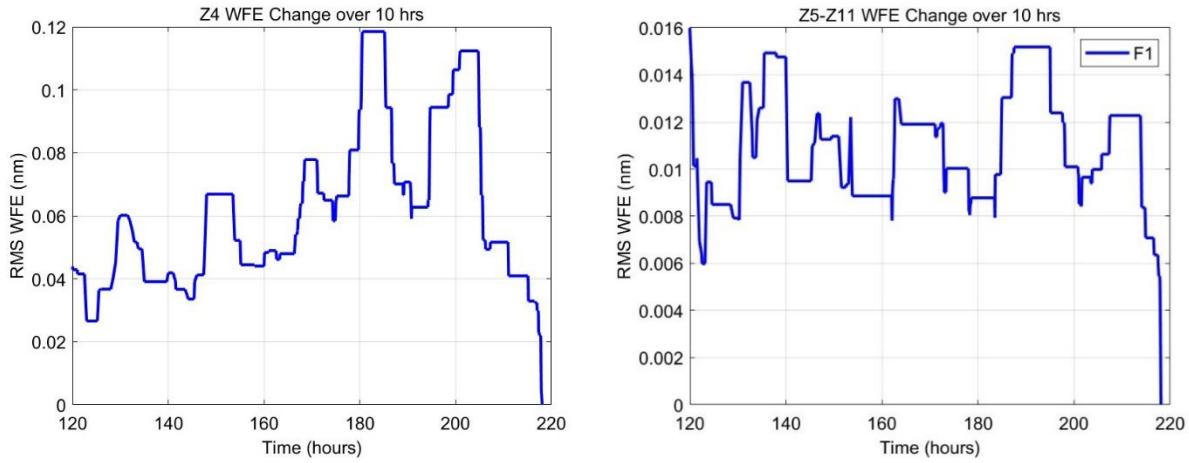

Figure 18 WFE changes at coronagraph channel over sliding 10 hour windows during the OS11 scenario. The figure on the left shows Z4 (defocus), while the figure on the right shows Z5-Z11 terms.

10. CONCLUSION AND SUMMARY

The Roman Optical Telescope Assembly was aligned at ambient temperature in a vacuum chamber, after which the telescope's optical performance, wavefront error, and pupil alignment were tested at cold operational temperatures in a thermal vacuum chamber. Both test campaigns were performed in double-pass test configuration, employing interferometry, Focus Diverse Phase Retrieval (FDPR), and Shack-Hartman Wavefront Sensing (SH-WFS) test techniques. Additionally, a new type of test, the Sinusoidal Thermoelastic Distortion Test (STDT) test, was performed during the TVAC test. The telescope's predicted On-Orbit, End of Life quasi-static optical wave front error performance is well within the 67.3 nm RMS requirement for the WFI channel and the 74.2 nm RMS requirement for the CGI channel. The result of the test campaign is a well-aligned telescope, stable to milliKelvin, and which has margin in the wave front error budget, and ample actuator range on-orbit throughout End-Of-Life.

After the completed test campaign, the telescope was delivered from L3Harris to NASA Goddard Space Flight Center, for integration of the two science instruments, spacecraft, and other flight hardware, after which the combined payload and space craft assembly will undergo final TVAC performance testing - measuring optical performance via FDPR using the SCM system - followed by observatory level environmental testing.

ACKNOWLEDGEMENTS

The authors would like to gratefully acknowledge the support and funding from NASA's Goddard Space Flight Center under the Roman Space Telescope project for funding this work.

REFERENCES

[1] Bert A. Pasquale, Thomas Casey, Catherine Marx, Guangjun Gao, Nerses Armani, David Content, John Hagopian, Alden Jurling, Clifton Jackson, Alice Liu, Art Whipple, Jacob Murray, "Optical design and predicted performance of the WFIRST phase-b imaging optics assembly and wide field instrument,", Proc. SPIE 10745, Current Developments in Lens Design and Optical Engineering XIX, 107450K (17 September 2018); doi: 10.1117/12.2325859

[2] D. Content, K. Aron, L. Abplanalp, K. Anderson, R. Capps, Z. Chang, J. Dooley, R. Egerman, R. Goullioud, D. Klein, J. Kruk, G. M. Kuan, M. Melton, J. Ruffa, M. Underhill, D. van Buren., "Wide-Field InfraRed Survey Telescope (WFIRST) 2.4-meter mission study." SPIE UV/Optical/IR Space Telescopes and Instruments: Innovative Technologies and Concepts VI. San Diego: SPIE Proceedings, 2013. 7.

[3] R. Hounsell, D. Scolnic, R. J. Foley, R. Kessler , V. Miranda, A. Avelino , R. C. Bohlin , A. V. Filippenko , J. Frieman S. W. Jha, P. L. Kelly, R. P. Kirshner, K. Mandel , A. Rest, A. G. Riess, S. A. Rodney , and L. Strolger, "Simulations of the WFIRST Supernova Survey and Forecasts of Cosmological Constraints". In: The Astrophysical Journal 867.1 (Oct. 2018), p. 23. doi: 10.3847/1538-4357/aac08b. url: https://dx.doi.org/10.3847/1538-4357/aac08b.

[4] Bente H. Eegholm, Catherine T. Marx, Victor J. Chambers, Jenny Chu, Guangjun Gao, Margaret Z. Dominguez, John P. Lehan, John G. Hagopian, Qian Gong, Laurie L. Seide, Evan Bray, Charles He, Jessica B. Patel, Manuel A. Quijada, Elliot Malumuth, Peter A. Morey, Martina S. Atanassova, Esben D. Jepsen, Jason R. Krom, Brian P. Kittle, Christopher Choi, Jonathan Salem, Linette D. Kolos, Hume L. Peabody, James J. Lyons, James A. Corsetti, Len Seals, Bert A. Pasquale, Maxime J. Rizzo, James E. Rhoads, Joshua E. Schlieder, Sangeeta Malhotra, Jeffrey W. Kruk, Arthur L. Whipple, David A. Content, Compact prism assembly for slit-less spectroscopy capability in Roman Space Telescope Wide-Field Instrument, *J. Astron. Telesc. Instrum. Syst.* **11**(2), 025001 (2025), doi: 10.1117/1.JATIS.11.2.025001. Roman Optical Telescope Integration Status and Preparation for Test

[5] Dominguez, Margaret Z; Eegholm, Bente H; Chambers, Victor J; Fincher, Wesley R; Gao, Guangjun; Gong, Qian; Hagopian, John G; Jepsen, Esben D; Lehan, John P; Marx, Catherine T; Seide, Laurie L, "Alignment and wavefront testing results of the Nancy Grace Roman Space Telescope Grism and Prism assemblies." 2023, Optical Fabrication and Testing, Paper# OM2B.2

[6] Peter Miller, Nicholas Ferry, Brian Martens, Dave Smith, Perry Voyer, and Tony Whitman "Roman Space Telescope: demonstration of integrated thermal control system test for the optical telescope assembly", Proc. SPIE 12188, Advances in Optical and Mechanical Technologies for Telescopes and Instrumentation V, 121881L (29 August 2022); https://doi.org/10.1117/12.2633215

[7] Matthew R. Bolcar, Josh Abel, Lisa Bartusek , Tom Casey, Bente Eegholm, Guangjun Gao, Tyler Groff, John Hagopian, Joseph Howard, Alden Jurling, Gary Kuan, Dave Kubalak, Alice Liu, Cathy Marx, Kim Mehalick, Mark Melton, Scott Rohrbach, Derek Sabatke, Tony Whitman, "The Roman Space Telescope Optical System: Status, Test, and Verification". Proc. SPIE 12676 (2023).

[8] Tony L. Whitman, Peter Miller, Joshua Abel, Bente Eegholm, Matthew Bolcar, J. Scott Smith, Brian Martens, Pete McCarthy, Joel Proebstle, and Erin Schiele "Roman optical telescope integration status and preparation for test", Proc. SPIE 12676, UV/Optical/IR Space Telescopes and Instruments: Innovative Technologies and Concepts XI, 126760P (4 October 2023); https://doi.org/10.1117/12.2679201